Influence of water surface roughness and incident light characteristics on multispectral reflectance of macroplastics

Tim van der Kuijl

January 2023

MSc thesis

Hydrology and Quantitative Water Management Group

Wageningen University

Abstract

Remote sensing is increasingly used to monitor floating plastics in riverine and marine environments, as it can increase monitoring scale spatially and temporally. Recent work has focused on detection of different plastic types in comparison to other items in the environment, such as vegetation and water. However, a major unknown is the effect of ambient conditions on the detectability of plastic items in riverine systems. Ambient conditions such as, water flow characteristics, submergence of items or weather conditions, can change the spectral signature of the plastics, other floating debris or the environment. This thesis studies the effect of light intensity, light angle and roughness of the water surface roughness, quantified by the Froude number, on the ability to distinguish plastic spectral reflectance values from vegetation and water. In a controlled laboratory and outside environments pristine and weathered plastic, riparian vegetation and water were scanned by a 9-band multispectral camera (MAIA-S2) under different light intensity, light angle and roughness of the water stream, quantified by the Froude number. A linear discriminant analysis determined important wavelengths to discriminate plastic from vegetation and water. A combination of spectral indices NDVI and NIDI had the highest performance, 81% of the plastic was correctly predicted, when tested by a Naïve Bayes algorithm to classify plastic, vegetation and water. Furthermore, increasing the Froude number had a strong significant negative correlation with classifier performance accuracy (Pearson's $r = -0.92$), while light angle and light intensity showed no significant correlation with classifier accuracy. Suggesting that the Froude number of the water has a considerable impact on the ability to discriminate plastic from vegetation and water. This study contributes to the effectivity of detecting floating plastics in the VIS-NIR spectrum and to the development of floating plastic detecting algorithms.

Contents

1 | Introduction

1.1 Context and motivation

Plastic pollution in riverine and marine systems is considered to be one of the main environmental challenges, as it provides a major challenge for the ecosystem (van Emmerik and Schwarz, 2020). Plastic waste accumulates in rivers by entering through natural drivers, such as wind and surface runoff (Bruge et al., 2018) or direct dumping (Mihai, 2018). Subsequently, these rivers transport plastic debris at an estimated rate of up to 4 million metric tons of plastic into the ocean per year. Other societal concerns are flood risks, entanglement and ingestion by animals (Gall and Thompson, 2015), or damage to vessels (McIlgorm et al., 2011). There is a need to find ways to monitor the plastic debris in river systems to gain insights into the scale of plastic pollution in these systems and the negative effect it has.

Efforts for data collection are increased recently, these efforts focus among others on collecting, monitoring, and classifying plastic debris. Al-Zawaidah et al. (2021) describes four sampling methods based on the accumulation of plastic in river systems; floating, riverbank, suspended, and riverbed plastics. Floating and riverbank research methods represent the dominant research categories. These in-situ methods consist of human visual counting (Van Emmerik et al., 2018), debris sampling using nets (Rech et al., 2014), and debris sample collection from existing infrastructure (Gasperi et al., 2014). These methods are labour intensive and are usually conducted over a limited time frame. This limits the capacity for interpreting the temporal rates of riverine macroplastic transport (Al-Zawaidah et al., 2021). Other methods are studied to scale up the monitoring capacity of riverine and marine plastics.

Remote sensing provides a set of methods to scale up the monitoring of floating plastic. Both spatially, harder-to-reach places can be monitored, and temporally, as it has the potential for more continuous and automated monitoring. Recent studies have focused on both airborne and spaceborne remote sensing. For example, Biermann et al. (2020) studied the ability to categorize floating litter based on spectral reflectance characteristics of different materials. Furthermore, Topouzelis et al. (2019) and Themistocleous et al. (2020) used large artificial plastic targets in coastal waters to investigate the applicability of Sentinel-2 imagery to distinguish plastic items. These studies used satellite data, a limiting factor for this approach is the spatial and spectral coarseness of the data. Resolutions from commercial satellite imagery, range from 1-5 meter (e.g. SkySat and RapidEye). Open-source satellite imagery, from the Sentinel-2A and 2B Earth Observation satellites by the European Space Agency (ESA), currently have spatial resolutions between 10-60m (Sentinel-2, n.d.). With these resolutions, it is hard to identify individual small-scale plastic objects. Plastic items in rivers are most often categorized as micro-, meso-, and macroplastics. The size of these plastics range respectively from $<$ 5 mm, 5 mm $<$ 5 cm, and $>$ 5cm (Blettler et al., 2017; Lebreton et al., 2018; van Emmerik and Schwarz, 2020). Close-range studies (imagery at $<$ 100 m distance) have been done in natural and laboratory environments. Cortesi et al. (2022) studied the ability to detect plastic on a river with a multispectral camera at different altitudes ranging from 20 to 80 meters. Knaeps et al. focused on the hyperspectral reflectance of dry, wet and submerge marine litter.

Previous studies, both outside and lab-based, utilized spectral signatures and used several remote sensing wavelength bands to create spectral indices. In 2014, Rokni et al. proposed several indices to extract water features. Among these NDVI, NDWI, NDMI, MNDWI and AWEI were tested for detecting plastic in water byThemistocleous et al. (2020) using multispectral data of plastic bottles obtained by the Sentinel-2 satellite and unmanned aerial vehicles (UAVs). They also introduced the plastic index (PI), based on red (665 nm) and near-infrared (842 nm) wavelengths, specifically to target the detection of plastic in water. PI values of plastic had the highest separation with water of these six indices. Using PI, with NIR and red wavelengths proved to be best to identify plastic bottles from water. Moreover, Biermann et al., 2020 proposed a novel index, the floating debris index (FDI), using data from the Sentinel-2 satellite. Besides indices-based approaches, approaches based on artificial intelligence are emerging (Cortesi et al., 2022; Balsi et al., 2021).

The variation in plastic spectral characteristics based on the imagery set-up such as indoor/outdoor, water conditions, artificial/natural lighting conditions and plastic deterioration rates, is still poorly understood. Furthermore, a challenge remains to confirm the reflection characteristics found in a laboratory setup for use in natural riverine environments (Martınez-Vicente et al., 2019). First, the potential current of the water in riverine and marine environments entails the movement of floating objects. This can lead to changing the appearance of these objects (Andriolo et al., 2022; Knaeps et al., 2021). Secondly, light conditions can change rapidly due to weather changes which force repeated sensor calibrations. Additionally, fluctuations in light conditions complicate the discrimination between plastics and other materials, such as vegetation. wood and sun glint. These sun glints (Mobley, 1999) and water characteristics such as waves, white caps (Dierssen, 2019), and bubbles (Hu, 2009) affect spectral signatures of water. Other external factors influencing the degree of plastic reflectance are wetting, submergence, and weathering (Garaba et al., 2021; Garaba and Dierssen, 2018). However, these effects are not investigated extensively and remain a knowledge gap for the detection of marine and riverine plastics.

These changing ambient conditions influence the ability to detect floating plastics and create biases in the data sets, because they are not sufficiently complete for all conditions. A need for unbiased balanced data sets is needed to increase the performance of machine learning techniques (Gnann et al., 2022). Within the challenges described the main focus of this study will be on three ambient conditions (1) water surface characteristics, (2) light conditions and (3) plastic degradation characteristics.

Water influences the effectivity to detect plastic with multispectral remote sensing in several ways. Garaba and Harmel (2022) demonstrated that submergence of the plastic items decrease the spectral reflectance of these items. Moshtaghi et al. (2021) discovered that the reflectance of water in near-infrared (NIR) wavelengths increases with turbidity, negatively effecting the performance to discriminate plastic from water. The effect of water surface roughness is on floating plastic reflectance and detection is currently poorly understood. Two causes of disturbance in the ability to detect plastic due to changes in the water surface roughness can be explained. First the effect on the plastic itself by submergence and second the change in spectral reflectance of the water itself. Water surface roughness effects the total reflectance and the but also the range of direction of this reflectance (Legleiter et al., 2017), thereby influencing the total reflectance a sensor captures.

Secondly, in natural environments light conditions fluctuate in intensity and incoming angle. The intensity and light angle both impact the outgoing reflectance rate of an item. Lower overall reflectance decreases the range between the highest reflectance and the lowest reflectance. This subsequently has an effect on ratios between wavelengths, decreasing the separation of index values between different objects and making it harder to detect plastic from other objects.

Thirdly, plastics occur in the environment in shapes, size and state of deterioration (Andriolo et al., 2021). Several previous studies have tested weathered plastic on their spectral reflectance (Garaba et al., 2021; Garaba and Dierssen, 2018; Moshtaghi et al., 2021). However, due to the complexity of the weathering process these studies observed contrasting outcomes. Garaba et al. found nearly identical absorption features for weathered plastic as for pristine plastics, while Moshtaghi et al. observed distinct spectral features. Further research is necessary to fully understand the impact of weathering on the spectral reflectance of plastic. Understanding the impact of these three ambient conditions on the spectral reflectance and the effectivity to detect natural conditions would be useful to improve the ability to monitor plastic with remote sensing techniques.

1.2 Research objective & research question

The objective of this study is to investigate the influence of four variables on plastic spectral characteristics and on the ability to discriminate plastic from riparian vegetation and water. Of these four variables, three relate to ambient conditions, namely: (1) water surface roughness, (2) light intensity, and (3) light angle. The fourth variable pertains to plastic items state of degradation. The main research question this study will answer is:

What is the effect of ambient conditions and plastic item characteristics and conditions on the ability to discriminate plastic from vegetation and water using multispectral imagery?

To help answer the main research question the following sub-questions will be answered:

- Which wavelengths are most effective to discriminate plastic from vegetation and water?
- Which spectral index has the highest performance to discriminate plastic from vegetation and water?
- What is the influence of water surface roughness, light intensity, and light angle on the ability to discriminate plastic from vegetation and water?
- What is the influence of plastic characteristics and condition on the ability to detect plastic?

1.3 Thesis outline

This thesis starts with the methods in chapter 2, which describes the experiments conducted to collect the data and the processing of the images and the analyses done with the collected data. In chapter 3 the results are presented and discussed, at the end of this chapter a synthesis and outlook is given. This is followed by a conclusion in chapter 4. Additional thesis data can be found in the appendices.

2 | Methods

For this study, data was collected by experiments done in the tilting flume of the Kraijenhoff van de Leur hydrology lab. Plastic items and vegetation in these experiments are scanned with a multi-spectral sensor, the MAIA-S2 sensor (engineering SRL; Eoptis SRL; Fondazione Bruno Kessler, 2017). The changing conditions, and variables, under which these scans were conducted are incident light (Lumen), light angle (degrees), and a measure for the roughness of the water stream and water surface. Water surface roughness is difficult to quantify on a river scale, in the research the Froude number was used, as it was a measurement for bulk flow characteristics such as waves and flow-depth interactions (Freeze et al., 2003). Nakayama and Yokojima, 2001 (2001) discovered that vertical fluctuations increase with Fr. Moreover, in a natural environment, the Fr of a river can be approximated with the discharge, cross-section, and width of the river at the study area.

In this chapter, the methodology is described (figure 2.1) starting with the collection of plastic items used in this study and scanning with the MAIA-S2 sensor. Furthermore, the general experiment setup will be explained as well as the four configurations of the setup used in this study. Lastly, the data processing is elaborated, consisting of image correction, manual pixel selection, and spectral analyses.

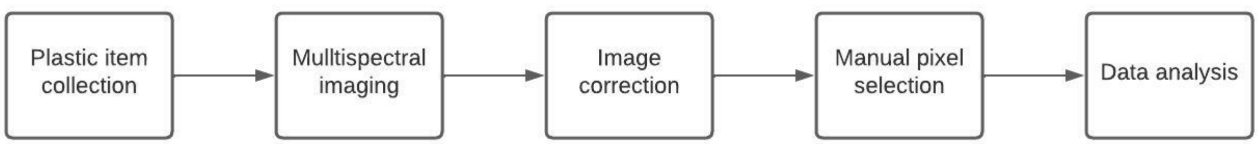

Figure 2.1: Flowchart of the methods in this study

2.1 Plastic item collection

Plastic items of various polymer types are found in or nearby river systems. In this study, six plastic polymer types (HDPE, LDPE, PS, PP, PET and ML) are used, based on their prevalence in river systems as floating plastic items (Erni-Cassola et al., 2019; van Calcar and van Emmerik, 2019). As they make up 65% of plastic production worldwide (PlasticsEurope, 2022). An overview of these polymer types can be found in table 2.1, describing their optical properties and examples of plastic items which are made with different polymer types. This study focuses specifically on plastic items that are found as (floating) plastics in or near rivers, other litters found in riverine systems such as submerged plastics, wood, and other litter are not included in this study.

Table 2.1: Types of plastic polymers used in this study with examples of use. (Barboza et al., 2019)

Type of plastic	Optical properties	Examples
Low-density polyethylene (LDPE)	(semi)transparent/coloured	cling film, garbage bags, shopping bags
High-density polyethylene (HDPE)	opaque/semitransparent white/coloured	milk bottles, detergent bottles
Polystyrene (PS)	opaque white/grey	plastic cutlery, food containers
Multi-layer (ML)	opaque coloured	chip bags, snack food packaging
Polypropylene (PP)	opaque white/coloured	drinking straws, yoghurt containers
Polyethylene terephthalate (PET)	(semi)transparent clear/coloured	soft drink bottles, clamshell packages

Both pristine plastics and plastics found at riverbanks, to be called weathered plastic, are used. The pristine plastics are plastics that have not been used and thus show no marks, these items are newly purchased. The weathered plastic items have been collected at the banks of the Nederrijn and Waal, appendix A.1 shows the location and date. The items are found and collected between the water line and the high water line. Slight degradation and weather marks, such as crumpling, scratching, and tearing, are present on the collected weathered items. For each plastic type named in table 2.1 both pristine and weathered plastic items are used in this study. The vegetation that is used is collected from the riparian zone of the Nederrijn near Wageningen. Figure (2.2) gives an overview of the items used for the experiments. The total number of plastic items is 38, of which 17 are pristine plastics (figure 2.2A) and 21 are weathered plastics (figure 2.2B).

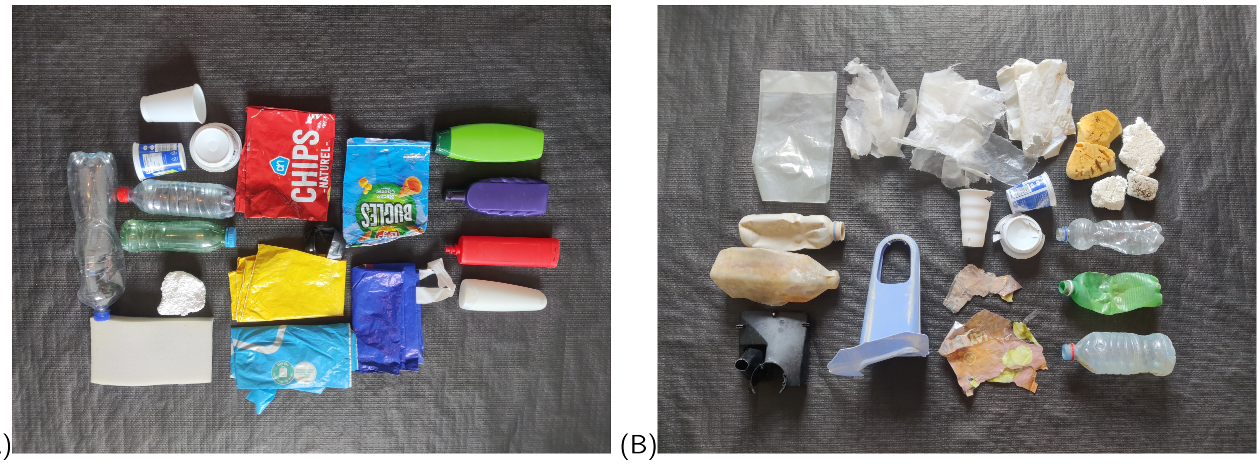

(A) (B)

Figure 2.2: Plastic collection used in this study with pristine plastic in figure A and weathered plastic in figure B

2.2 Multi-spectral imaging

2.2.1 MAIA-S2 sensor

The multispectral imaging of plastic, vegetation and water was performed by the MAIA-S2 sensor, a nine-band multi-spectral sensor in the visible and near-infrared wavelength range. These nine bands have wavelength intervals similar to the ESA Sentinel-2 MSI satellite, which has been used as a potential tool for floating plastic monitoring (Garaba et al., 2021; Ciappa, 2021; Kikaki et al., 2020). The wavelength intervals for both the MAIA-S2 sensor and the Sentinel-2 satellite are detailed in table 2.2. Besides the wavelength range corresponding with the Sentinel-2 satellite bands, this sensor has several other advantages for monitoring plastics in riverine environments. The sensor is applicable for both drone and static imagery, which allows for monitoring in both accessible and less accessible locations in riverine systems. During these experiments the sensor was only used for static imagery. Another advantage is the exposure time of the MAIA S2 sensor which ranges from 0.1 ms to 50 ms (typical 1ms). This short exposure time makes this camera better suited for in field high resolution measurements than hyperspectral cameras, which have typically a longer exposure time. However, this sensor has a shortcoming as well which have to be considered. First, the wavelength range of the sensor is not suited for some spectral indices used in other studies to detect floating plastics (Biermann et al., 2020). Furthermore, P. Tasseron et al. (2021) showed that wavelengths best suited to distinguish various plastic polymer types with certainty are within the short-wave infrared (SWIR) ranges of the spectrum.

Table 2.2: Wavelength intervals of the MAIA-S2 Bands and corresponding Sentinel-2 MSI band

MAIA-S2 band	Color	Start WL (nm)	Stop WL (nm)	Central WL (nm)	Corresponding Sentinel-2 band
B1	Violet	433	453	443	B1
B2	Blue	457.5	522.5	490	B2
B3	Green	542.5	577.5	560	B3
B4	Red	650	680	665	B4
B5	Red Edge 1	697.5	712.5	705	B5
B6	Red Edge 2	732.5	747.5	740	B6
B7	NIR 1	773	793	783	B7
B8	NIR 2	784.5	899.5	842	B8
B9	NIR 3	855	875	865	B8a

2.2.2 Experiment setup

To study the different variables a total of four experiments were performed. In table 2.3 an overview is given of the different experiment setups. Experiments 1 and 2 were executed in a dry environment. The items were scanned in front of a dark paper background. Experiment 3 and 4 were executed in a wet environment in which the items are being scanned while floating in water. The standard light angle of 80 degrees is used in all experiments with the exception of experiment 1. In this experiment, plastic is scanned under various incident light angles between 60-90 degrees to the surface. Furthermore, the standard illumination of experiments 1 and 4 is 1500 (Lumen). In contrast to the other experiments, the images of experiment 4 have been scanned one item at a time instead of multiple items at once. Due to the flowing water, it was not possible to position multiple items in the image frame. As a consequence, the number of images were higher for experiment 4 than for experiments 1,2, and 3.

Table 2.3: Overview of the various configuration of the experiment setup. *For a light angle of 80 degrees the data from Illumination (dry) 1200 Lumen is used. ** For 0.0 Fr the data from Illumination (wet) 1500 Lumen is used.

Experiment	Studied variable	Range of parameter change	Step size	Total number of images
1	Light Angle (dry)	60 – 90 (degrees)*	10 degrees	39
2	Illumination (dry)	600 – 1500 (Lumen)	300 Lumen	52
3	Illumination (wet)	600 – 1800 (Lumen)	300 Lumen	65
4	Froude Number (wet)	0 – 1.2**	0.2	234

The experiments were executed in a tilting flume of the Kraijenhoff van de Leur laboratory of the Wageningen University. This flume has a length of 17 meters, a width of 1.2 meter, and a maximum water depth of 0.5 meter. The discharge, 0-100 L/s, and the incline, 0-4%, were adjustable and were used to change the water flow. Figure 2.3 gives an overview of the general experiment setup. Fixed on top of the flume is the Maia-S2 sensor with ILS sensor on a scaffold. To ensure consistent illumination for the duration of a run, a halogen light was fixed to a scaffold opposing the Maia-S2 sensor. This general setup is the core setup for the all the experiments of the different variables studied. The sensor captures the images at a 0 degree nadir angle, perpendicular to the surface. With a wifi connection to the Maia-S2 sensor, a computer could configure parameters and take images of the plastic with a web interface linked to the sensor. To ensure the (floating) items were captured within the image frame, the sensor was set to acquire images with a frequency of 4 images per second.

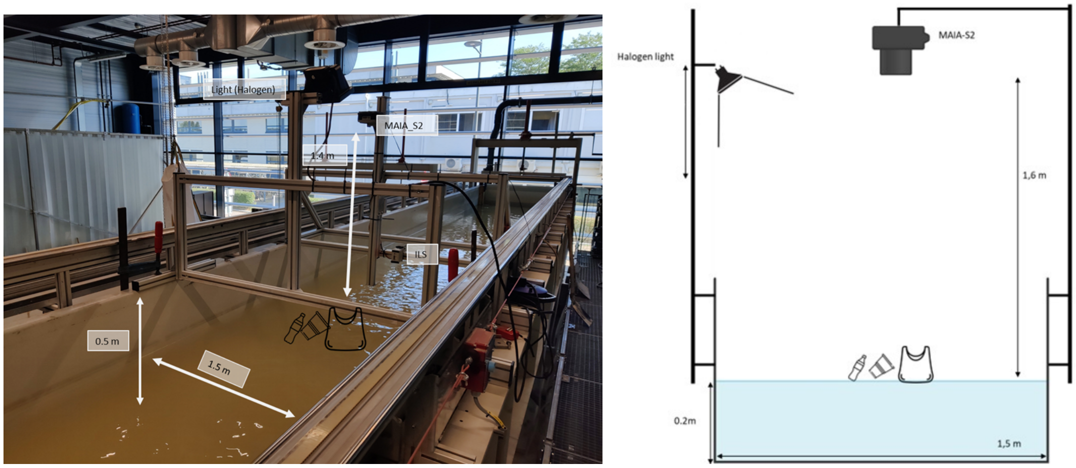

Figure 2.3: (A) An overview of the experiment setup within the tilting flume. (B) a schematic overview of the experiment setup for the wet experiments, dry experiments have a similar setup without water.

Changes in light angle and illumination was carried out by altering the position and brightness of the halogen light respectively. The roughness of the water surface does not have a direct quantitative measure. So to quantitatively represent the water surface roughness the Froude number (Fr) was used. This dimensionless number describes flow regimes of open channel flow. Floating plastic debris is most common in lowland riverine systems, as river plastic quantities show high correlation with population density and urbanization (Best, 2019). Near these lowland systems the population density of humans is larger. Fr in these rivers ranges from 0 to 2, and most commonly between 0 to 1 (Ferrick, 1985). With the following equation 2.1 Fr is calculated for open channel flow.

$$Fr = \frac{V}{\sqrt{gD}} \tag{2.1}$$

Where V is flow velocity (m/s) and g is the gravitational acceleration $(9.81m/s^2)$. The hydraulic depth (D) is the ratio the cross-sectional area,A (m^2), to the width of the flume W (m). Flow velocity was calculated by dividing the discharge, Q (m^3/s), by the cross-sectional area of the flume. Incorporating the hydraulic depth from the flume dimensions and the flow velocity from the discharge of the flume the Fr is calculated by the equation 2.2.

$$Fr = \frac{Q/A}{\sqrt{g\frac{A}{W}}} \tag{2.2}$$

To change Fr at the image area the discharge of the flume and the water depth were changed. The flume was rectangular therefore the water depth was consistent over the entire width. Fr was changed using equation 2.2, by altering the water height by raising and lowering a weir at the end of the flume and changing the discharge of the flume.

2.3 Data preparation

After all the experiments were executed the images were processed with the MAIA - MultiCam Stitcher Pro software to process the images from the MAIA-S2 sensor. From all the images captured, a set of images displaying plastic items and representing all the experiment setups and containing all the plastic and vegetation types was manually selected for data analysis. This set of images is converted to relative reflectance data, to optimize the signal-to-noise ratio. This was done using the reflectance values of a white reference and a dark reference. Based upon the approach of ElMasry and Sun, referring to equation 2.3:

$$I = \frac{(I_0 - D)}{(W - D)} \tag{2.3}$$

Where I is the relative reflectance image, I_0 is the raw image, and W and D are respectively the white and dark references. These references were collected by a white sheet as a white reference and the black background as a dark reference. The common practice to capture the dark reference of closing the aperture of the camera, so that no light is striking into the sensor, was not possible. The data pre-processing with the built-in software of this sensor did not allow for images with low reflectance. Therefore the dark reference image was captured by a black sheet. For the experiments that did not change the illumination or light angle the same reference image is used. When the illumination levels were changed a reference image that was representative of that illumination level was used.

2.4 Manual pixel selection

Using the PerClass machine learning toolbox (perClass BV, n.d.) in MATLAB representative pixels were manually annotated into five classes; (1) all plastics combined, (2) pristine plastics, (3) weathered plastics, (4) vegetation, and (5) water. All six polymer types discussed in table 2.1 were incorporated in the classes 1,2, and 3. The combined plastic class included the pixels from both the pristine and weathered plastic classes. These classes were annotated for all data from the different experimental runs. In table 2.4 an overview of the classes is shown including the number of items and total number of pixels per wavelength band. During this study, class 1 was used to investigate into the performance of indices and the effect (section 3.2) of the ambient conditions (section 3.3). Classes 2 and 3 were used to investigate the differences between pristine and weathered plastics (section 3.1) and for the analysis of effect of plastic deterioration (section 3.4) on the effectivity to discriminate plastic from vegetation and water.

Table 2.4: An overview of the items used in the study, and the number of pixels per wavelength band for each class.

Class	Items	Total pixels per bands (#)
(1) Plastic	38	5567152
(2) Pristine plastic	18	3197980
(3) Weathered plastic	20	2369172
(4) Vegetation	9	246501
(5) Water	NA	667558

2.5 Data analysis

2.5.1 Spectrum analysis

In total 6.5 million pixels were sampled for all classes and experiments for each wavelength band of the sensor. Due to the large number of pixel a spectral signature was extracted with the mean and standard deviation of the pristine and weathered plastic, vegetation, and water classes. Furthermore, a Fisher's linear discriminant analysis (LDA) (Fisher, 1936) was calculated to show the importance of each wavelength in the separation of plastic pixels from vegetation and water. The LDA describes the relative contribution to the variance of reflectance signatures between two classes. Higher levels of LDA weights imply larger contributions of these bands in the separation of two classes. LDA is widely used to lower high-dimensional data to two dimensions without losing the variation between two classes. The linear discriminant is based on maximizing a ratio of between-class variance to within-class variance with the goal of reducing data variance in the same class and increasing the separation between classes (Li and Wang, 2014). The between-class variance S_B

is the difference between the mean values of two classes (equation 2.4). The within-class variance S_W is the difference between each value and the mean of that class (equation 2.5). Combining these equations and maximizing the ratio, will result in Fisher's linear discriminant $J(w)$ (equation 2.6). Where m_1 and m_2 are the mean values of a class, x_i individual values of a class, and w the weights vector.

$$S_B = (m_1 - m_2)(m_1 - m_2)^T \tag{2.4}$$

$$S_W = \sum_{i \epsilon c}(x_i - m_1)(x_i - m_1)^T + \sum_{i \epsilon c}(x_i - m_2)(x_i - m_2)^T \tag{2.5}$$

$$J(w) = \frac{w^T S_B w}{w^T S_W w} \tag{2.6}$$

2.5.2 Naive Bayes classifier

To study the ability of indices and the effect of the ambient conditions and plastic variables a Gaussian naive Bayes classifier was used. This classifier was trained with the Classification Learner application in MATLAB (The MathWorks, 2013), leveraging Bayes Theorem (Leung, 2007). The classifier used the following procedure. First, the classifier estimates the densities of the predictors within each class by computing the class-specific weighted mean and the unbiased estimate of the weighted standard deviation. Second, the classifier posterior probabilities are calculated according to Bayes rule with equation 2.7. Where Y is the random variable corresponding to a class of an observation, $X_1, ..., X_n$ are the random predictors of an observation and $\pi(Y = k)$ is the prior probability that a class is index k.

$$\hat{P}(Y = k|X_1, ..., X_n) = \frac{\pi(Y = k)\prod_{j=1}^{P} P(X_j|Y = k)}{\sum_{k=1}^{K} \pi(Y = k)\prod_{j=1}^{P} P(X_j|Y = k)} \tag{2.7}$$

The pixels were manually annotated (section 2.4), thus for each pixel in the database the true class was known. The classifier was trained for 60% of the data (Dobbin and Simon, 2011; Picard and Berk, 1990). Next, the classifier was tested on the other 40% of the data for accuracy (ACC), recall (RE) and precision (PR). This train and test set ratio was used throughout all classifier calculations in this study. The specific data sets to train and test the classifier differed depending on the analysis performed, this is mentioned in the relevant sections. The spectral indices were the parameters of the algorithm, so based upon the number of indices the classifier had one or two parameters. With the exception of the nine band spectrum which used all nine wavelength bands as parameters. The input classes used were (1) all plastic combined, (4) vegetation and (5) water for the analysis in sections 3.2 and 3.3. In section 3.4, classes (2) pristine plastic, (3) weathered plastic, (4) vegetation and (5) water are used.

Next, the trained classifier predicted the annotation of classes for the pixels of the test data set. To determine the performance a confusion matrix was constructed. From this confusion matrix the ACC of the entire classifier was calculated as well as the RE and precision PR of plastic, vegetation, and water. The ACC was calculated as the total number of correct predictions divided by the total number of a data set (equation 2.8). In which TP are the true positives, the pixels that are correctly predicted as true observations and TN are the true negatives, pixels that are correctly predicted as false observations. P and N are the total correctly and falsely predicted observations respectively.

$$ACC = \frac{TP + TN}{P + N} * 100 \tag{2.8}$$

The RE was calculated by equation 2.9 and describes the probability of a model that an observation with a true outcome is predicted as a true predicted outcome. In which FN are the false negatives, the pixels that are falsely predicted as true observations by the classifier.

$$RE = \frac{TP}{TP + FN} * 100 \tag{2.9}$$

The PR was calculated by equation 2.10 and described the probability that an observation with a true positive predicted outcome actually has a positive outcome. In which FP are the false positives, the pixels that are falsely predicted as true observations.

$$PR = \frac{TP}{TP + FP} * 100 \tag{2.10}$$

2.5.3 Spectral Indices

A comparison is made of the ability of 8 spectral indices to distinguish plastic from vegetation and water. The indices that are tested are all containing the wavelengths with the largest variability between plastic, vegetation and water as calculated by the LDA. The indices have been used to detect plastic in previous studies (Cortesi et al., 2021; Rokni et al., 2014; Themistocleous et al., 2020), and contain wavelengths that have the highest LDA weights, red (665 nm), red-edge (740 nm), and NIR (842 nm). Table 2.5 shows a detailed depiction of these wavelengths.

Table 2.5: Overview of the indices evaluated in this study

Index	Algorithm	Reference
9 band spectrum	(-)	This report
EVI: Enhanced vegetation index	$EVI = 2.5(\frac{(\rho_{NIR} - \rho_{red})}{(\rho_{NIR} + 6\rho_{red} + 7.5\rho blue + 1)})$	Liu and Huete, 1995
NDWI: Normalized different water index	$WDVI = \frac{(\rho_{green} - \rho_{NIR})}{(\rho_{green} + \rho_{NIR})}$	Rokni et al., 2014
NDVI: Normalized difference vegetation index	$NDVI = \frac{(\rho_{NIR} - \rho_{red})}{(\rho_{NIR} + \rho_{red})}$	Rouse et al., 1974
PI: Plastic index	$PI = \frac{\rho_{NIR}}{(\rho_{NIR} + \rho_{red})}$	Themistocleous et al., 2020
NIDI: Normalized infrared difference index	$NIDI = \frac{(\rho_{NIR} - \rho_{red-edge})}{(\rho_{NIR} + \rho_{red-edge})}$	Vescovo et al., 2012
NDVI + NIDI	$NDVI + NIDI$	This report
NDVI + NDWI	$NDVI + NDWI$	This report

.

2.5.4 Influence of ambient conditions and plastic variability

To analyse the influence of the ambient conditions, Fr, illumination in both wet and dry circumstances and the light angle, a naive Bayes classifier was used as well. This classifier was trained using both NDVI and NIDI data, which had the highest performance of all indices tested. The accuracy of the classifier was 91% against other indices which had 86% accuracy or lower, further elaboration can be found at section 3.2. The classifier was trained with data from the lowest value of each of the four variables and tested for each value of that specific variable. For example, to analyse the influence of Fr the classifier was trained for Fr 0.0 and tested for each of the Fr values. The accuracy of the entire classifier was calculated together with the RE and PR of plastic, vegetation, and water, for each value of the ambient conditions. A Pearson and a Spearman correlation between the accuracy of the classifier and ambient condition values were tested. The Pearson correlation examines the linear relation between two variables and the Spearman correlation is used to examine a non-linear relation between two variables. The classifier approach is repeated for a classifier trained for the entire data set to include a larger variety of values for each class, instead of training the classifier for one specific situation.

Similarly, a Naive Bayes classifier is used to test the influence of plastic characteristics and conditions. Hereby a comparison is made between a classifier trained for pristine plastics and a classifier trained for weathered plastics, by testing the performance of both classifiers on a pristine and a weathered plastic data set. An analysis of the specific effect of different plastic polymer types will not be conducted in this study. Because discrimination of specific polymer types is difficult in the VIS-NIR (400-900 nm) wavelength range used in his study, since specific polymer absorption features are found at wavelengths $>$900 nm (Garaba and Dierssen, 2020; P. Tasseron et al., 2021).

3 | Results & Discussion

3.1 Spectral variability and linear discriminant analysis

Differences in mean value and standard deviation were found comparing the spectral signature of water, vegetation, pristine plastics, and weathered plastics (figure 3.1). Spectral signatures found for water and vegetation show characteristics similar to signatures found in previous studies (Corbari et al., 2020; Themistocleous et al., 2020). The water reflectance values were close to zero for the entire spectrum and decreased with larger wavelengths. The vegetation reflectance had a sharp increase in spectral reflectance from 700 nm to 780 nm, caused by the internal cell structure of leaves (Meacham-Hensold et al., 2019).

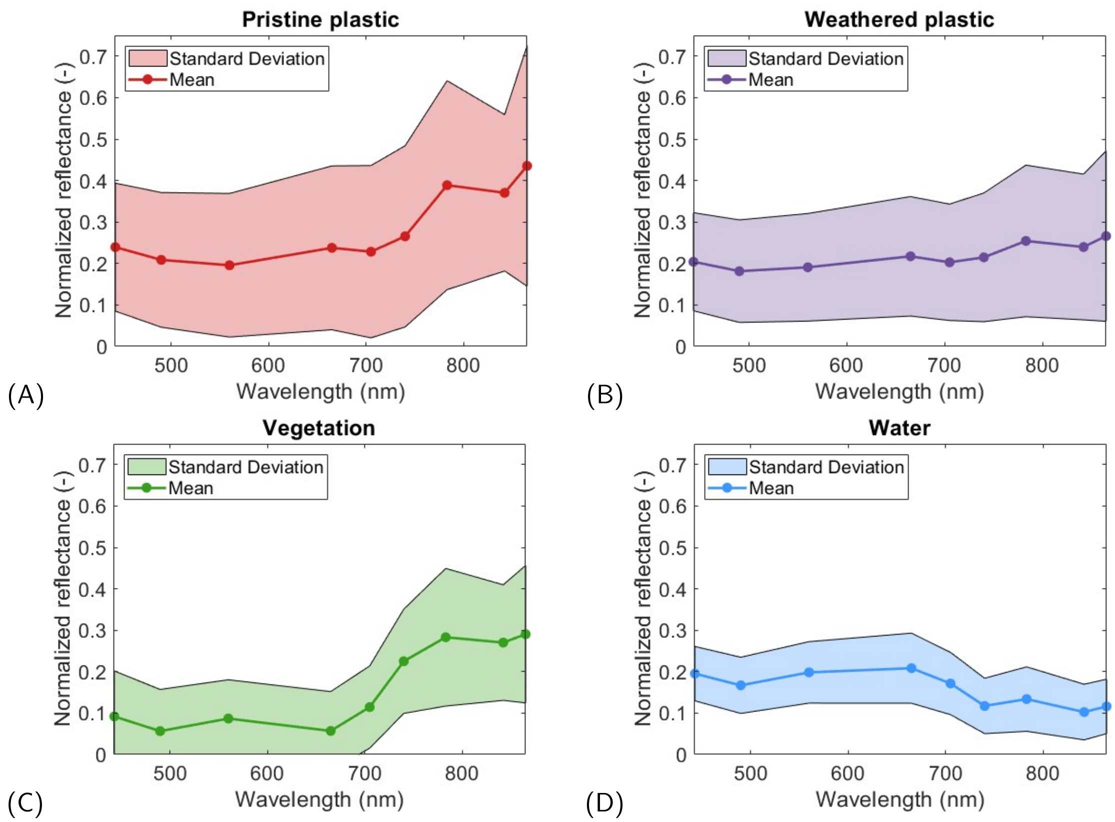

Figure 3.1: Mean and standard deviation of the normalized reflectance spectra of (A) Pristine plastic, (B) weathered plastic, (C) vegetation, and (D) water.

The standard deviation of plastics, both pristine and weathered, was high in comparison to the standard deviation of vegetation and water. A likely cause is the use of different polymer types, which have differences in individual reflection spectra (Iordache et al., 2022). Overall the spectral signature of pristine plastics shows good agreement with previous studies (P. Tasseron et al., 2021; Corbari et al., 2020), characterized by a small dip at 710 nm followed by an increase at 750 nm. The reflection characteristics of weathered plastics were more stable for different wavelengths. Differences in the standard deviation between pristine and weathered plastics is likely explained by differences in the collected items of weathered plastics and pristine plastics used in the study. The sampled pristine plastics and weathered plastics differed in size, shape, and apparent colour. The size and shape of an item influences the susceptibility of that item to water conditions. A thin sheet plastic is more prone to be effected by waves in the water than a PET bottle. As a consequence the item can submerge affecting the spectral signature of the item (Garaba and Harmel, 2022). Apparent colour affects the spectral reflectance in the visual wavelength range (400-800 nm) (Moshtaghi et al., 2021).

The distinctly different spectral reflectance of plastics, vegetation and water resulted in high and low LDA weights for different wavelengths. Wavelength 842 nm gave high LDA weights for plastic and water. For plastic with vegetation LDA weights peaked at 665 nm and 740 nm. Figure 3.2 shows the LDA weights, describing the ability of each wavelength to discriminate between pristine and weathered plastics and water (A) and vegetation (B). The LDA weight for plastic and water varied between pristine and weathered plastic. Pristine plastic weights had a large peak at 842 nm indicating that pristine plastic and water had the largest separation of spectral reflectance at that wavelength. In contrast, LDA weights for weathered plastic and water peaked at four wavelengths, 560, 665, 740, and 865 nm. However, LDA weights in the visible wavelength range 400-700 nm are considered to be of less importance because the reflection of these wavelengths is strongly influenced by the apparent color of the item (Garaba et al., 2021). This results in varying LDA weights depending on the collection of sample items. These findings correspond with the findings of P. Tasseron et al. (2021), who showed that for the Sentinel-2 B6 (740 nm) were powerful for discriminating water and floating debris and Biermann et al. (2020) suggested that B8 (842 nm) is key for the detection of floating debris in coastal waters. A large variation between the LDA weights of pristine plastics and weathered plastic exists at 842 nm. The LDA weight for pristine plastic is twice that of weathered plastic, which is expected considering the difference in spectral reflectance of these items (figure 3.1(A & B)). Pristine plastic had a mean spectral reflectance of 0.37, and a standard deviation of 0.19 at 842 nm. Whereas weathered plastic had a mean reflectance of 0.24, and a standard deviation of 0.18 at that wavelength. The spectral reflectance of water was 0.1 at the same wavelength. Therefore the difference between the reflectance of water and pristine plastics is larger than the difference between water and weathered plastic at 842 nm. This leads to a higher LDA weight, as the LDA weight is calculated by the difference of the means between two classes divided by the variance within the classes.

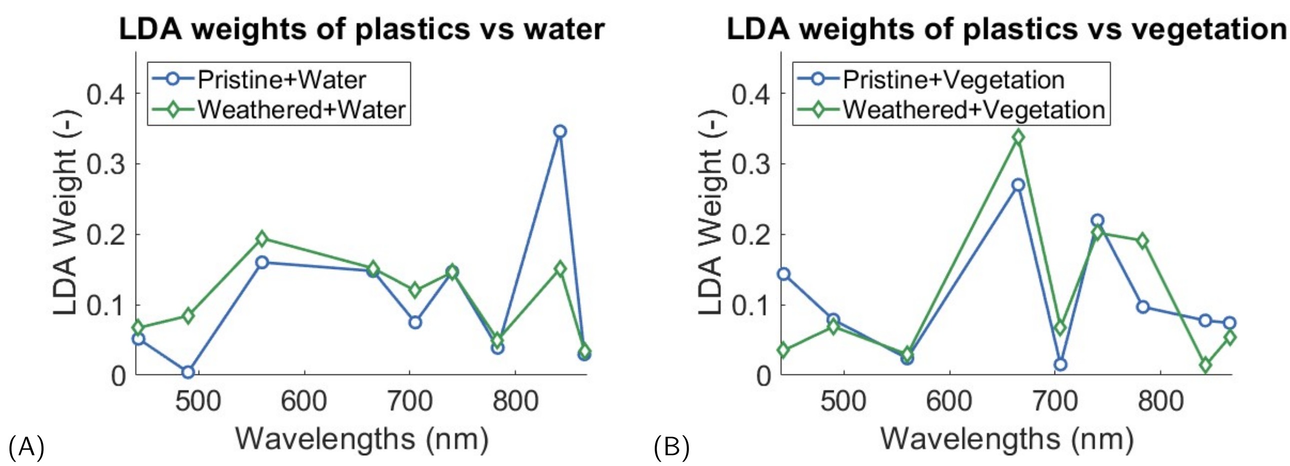

Figure 3.2: LDA weights of reflectance values of pristine and weathered plastics with water (A) and vegetation (B). The dots represent the different bands (B1-B9) of the MAIA-S2 camera depicted on their respective wavelengths

The LDA of pristine and weathered plastic with vegetation had similar results with both the highest LDA weights at 665 nm and 740 nm. The peak of weathered plastic was slightly higher than that of pristine plastic, this is expected to be caused by differences in plastic sample collection since reflection is dependent on the apparent color in this wavelength range. The LDA weights correspond largely to results demonstrated by P. Tasseron et al. (2021), who showed high LDA weights for Sentinel-2 bands, B4,B5 and B6 corresponding to respectively 665, 705, and 740 nm. However, in contrast to P. Tasseron et al. low LDA values had been found for 705 nm. This wavelength is located in the red-NIR transition of vegetation reflectance, therefore difference is vegetation samples could lead to difference in reflectance. Subsequently causing the LDA weight to differ.

Combining results for plastic with water and plastic with vegetation, wavelengths 665, 740 and 842 nm are most important to discriminate plastic from water and vegetation. These wavelength correspond to MAIA-S2 bands B4,B6 and B8. Indices utilizing these wavelengths are expected to discriminate plastic best from vegetation and water. In the next section this will be tested with Naive Bayes classifications trained for eight different indices or index pairs.

3.2 Spectral indices

In table 3.1 the accuracy of these Naive Bayes classifiers evaluated on a test data set is displayed. For this classification all plastic combined, vegetation and water are used as prediction classes. The total accuracy of the classifier is depicted, as well as the RE and the PR of plastics. Classifiers trained for indices NDVI and PI were most accurate for classifiers trained for one index. The classifier had an accuracy 86% for these two indices. This accuracy is 7% higher than the accuracy of the classifier using the reflectance values of all nine bands scanned, demonstrating the importance of distinct spectral signatures to detect objects (Topouzelis et al., 2019; Topouzelis et al., 2020). NDVI and PI are comprised of red (665 nm) and near-infrared (842 nm) wavelengths confirming the importance of these wavelengths for the separation of plastic, vegetation and water pixels. This is in agreement with the LDA weights previously demonstrated.

Table 3.1: Overview of the accuracy of the trained Naive Bayes classifiers. As well as the RE and PR of the prediction of plastic.

Index	Accuracy (%)	Plastic RE (%)	Plastic PR (%)
9-band spectrum	79	48	83
EVI	33	0	100
WDVI	79	49	84
NDVI	86	66	90
PI	86	66	90
NIDI	67	26	76
NDVI + NIDI	91	81	92
NDVI + WDVI	86	67	88

Other indices have lower classifier performance separating plastic, vegetation and water. WDVI, which uses besides NIR wavelengths green wavelengths (560 nm), had similar to the 9-band spectrum an accuracy of 79%.. EVI, which besides NIR and red wavelengths uses blue wavelengths (490 nm), had an accuracy of 33%. Both indices have lower performance than NDVI and PI, confirming that green and blue wavelengths show less potential to distinguish plastic, vegetation and water. However this could be influenced by the color of the sampled items in this study as discussed before (3.1).

NIDI, calculated with Red-Edge (740 nm) and NIR (842 nm) wavelengths, had an accuracy of 67%, 19% lower than the accuracy off NDVI and PI. Despite the fact that both wavelengths were found to be important in the separation of plastic, vegetation and water. However, the LDA weights of plastic and vegetation which were higher for red wavelengths (0.32) than for red-edge wavelengths (0.25) (figure 3.2B). Subsequently, the vegetation is overpredicted at a higher rate than water with NIDI. The PR for vegetation is 57%, stating that 57% of pixels predicted as vegetation are actually vegetation. Meanwhile 89% of the true vegetation is predicted correctly as vegetation (RE), causing a difference of 32% between RE and PR. This effect did not occur as strongly for water, since the difference between RE and PR was 8%. Given the high RE of water and the low RE of plastic, this overprediction of vegetation is caused by a misclassification of plastics. In contrast to NIDI, the difference in PR and RE for NDVI was similar for vegetation (12%) and water (11%). Confirming that red wavelengths were better to discriminate plastic from vegetation than red-edge wavelengths.

However, a classifier trained with NDVI and NIDI as parameters increased the ACC with 5% to 91%. A combination with PI and NIDI had similar results. Combining two indices proves to be a promising approach to discriminate plastic vegetation and water. Similarly, Biermann et al. (2020) found that examining two indices together is a promising method to discriminate plastic from marine materials, including seaweed, water, timber and foam. As these materials showed distinct clustering when examined for floating debris index (FDI) and NDVI together. In agreement with the lower LDA weights for green wavelengths, combining NDVI and WDVI did not increase the accuracy of the classifier in comparison with the classifier trained for only NDVI.

Next, the performance of the classifier to predict plastic was examined. The RE of plastic is consistently lower than the overall accuracy of the classifier. As was expected due to the high standard deviation of plastic compared to vegetation and water. For NDVI an PI 66% of the true plastic pixels is correctly predicted as plastic. The FN of plastic are predicted both as vegetation and water at similar rates. The RE of vegetation and water is with, 93% and 99% respectively. But for both classes the PR is lower indicating an overprediction of these classes, resulting in a decrease in the overall accuracy of the classifier. Combining NDVI and NIDI in the classifier increases the RE of plastic to 81%. Vegetation increases to 99%, but water decreases slightly to 93% and for both classes an slight increase in PR (appendix A.2). The performance of the classifier with both NVDI and NIDI is promising and shows similar levels of performance to automated classifier used in previous studies (Acuña-Ruz et al., 2018; Sannigrahi et al., 2022). However a direct comparison is complicated. These classifier were performed for more classes and for far-range imagery, which generally have lower standard variation than high resolution close-range imagery used in this study. Which decreases the overall performance of a classifier (Chen* et al., 2004).

In figure 3.3 a visualization is shown of the Naive Bayes classifier performance, for pristine HDPE plastics in standing water. Figure 3.3A is an RGB image to show the true pixel representation. In the image only HDPE plastics and water is present, in the bottom center water glints are present. In both figure 3.3B, the NDVI-trained classifier, and figure 3.3C, NDVI + NIDI-trained classifier, the majority of the plastic item pixels were predicted correctly. However, near item borders and relief within the plastic items pixel were predicted as vegetation or water. The visualization displays results comparable with the RE and PR findings previously discussed. The NDVI-trained classifier performed slightly better separating plastic and water. Especially the most right sample item is better predicted by the NDVI classifier. However, the NDVI classifier predicted more plastic pixels as vegetation than the NDVI + NIDI classifier. Meanwhile water was overpredicted for the NDVI + NIDI-trained classifier. Furthermore, most of the water is correctly predicted as water, however near the water glints the prediction was less accurate (Topouzelis et al., 2019). Especially the NDVI + NIDI-trained classifier incorrectly predicted these pixels as plastic.

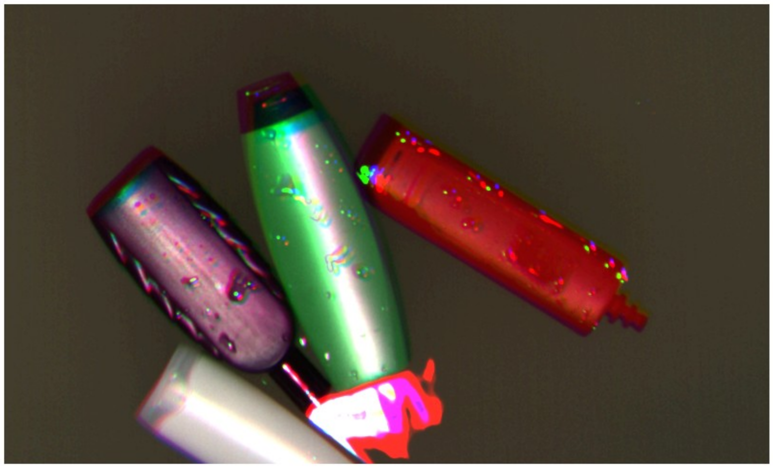

(A)

(B)

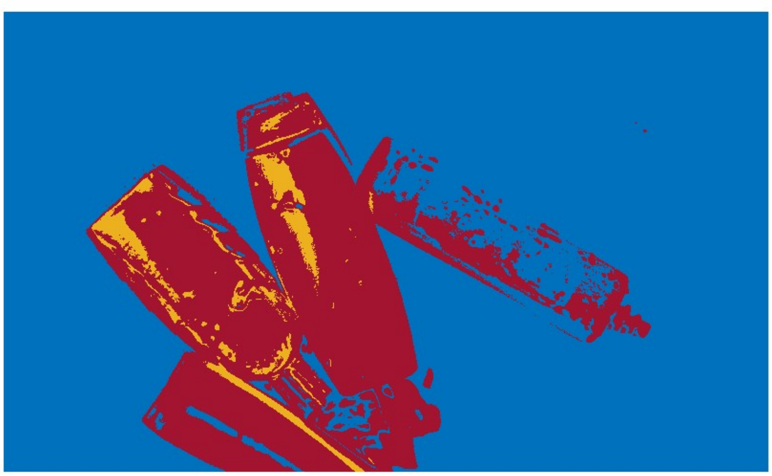

(C)

Figure 3.3: Visual representation of the classifier performance for pristine HDPE plastics under standing water conditions with 1800 Lumen of light.(A) RGB image (B) Naive Bayes NDVI prediction (C) Naive Bayes NIDI-NDVI prediction. The classifier was trained for three classes; plastic (red), vegetation (yellow) and water (blue).

3.3 Influence of ambient conditions

Increasing Fr had a large negative effect on the performance of classifier, this indicates that Fr variation effects the ability to detect plastic. Table 3.2 depicts a Pearson and Spearman correlation between the four variables and a Naive Bayes classifier trained on the NDVI and NIDI data of the lowest value for each variable. The Pearson and Spearman correlation between Fr and the classifier performance had a very strong negative correlation of -0.92 and -0.96. The p-value for both correlations was <0.01 indicating strong evidence against the null hypothesis and thus statistically significance. The classifier performance for varying wet and dry illumination levels and light angle had moderate to strong correlation but have no significance with p-values larger than 0.05. Although the p-value of illumination in the dry situation is close to significance, as 0.08 was close to 0.05, the correlation is deemed insignificant because of the small number of variable data points. This could lead to both an underestimation or an overestimation of the significance. Besides the relatively small amount of data points, the dry illumination data could be influenced by the experiments both done inside and outside. Differences in setup, light source and camera position could have an effect on the results. No significant correlation was found when calculated for the varying illumination levels inside and outside separately (appendix A.2). Appendix A.3 presents an overview of the classifier performance for all ambient conditions is presented, where the accuracy of the classifier and the RE and positive predictive value of plastic, vegetation, and water can be found.

Table 3.2: Correlation between ambient conditions and NDVI-NIDI trained Naive Bayes classifier

Ambient condition	Pearson correlation r	Pearson correlation p	Spearman correlation r	Spearman correlation p
Froude number	-0.92	<0.01	-0.96	<0.01
Illumination (Wet)	-0.53	0.36	0.00	1.0
Illumination (Dry)	-0.76	0.08	-0.6	0.24
Light angle	-0.58	0.42	-0.8	0.33

In table 3.3 an overview of the classifier accuracy, and corresponding plastic RE and PR are described. The classifier performance decreased sharply at Fr 0.4 from 91% to 58%, after this the accuracy had a slightly decreasing trend with increasing Fr. Although the RE of the classifier to predict plastic has an increasing trend this is in all probability contributed to an over-prediction of plastics which is indicated by the sharp decrease in PR at Fr 0.4 and higher. Figure 3.4 presents a confusion matrices of the classifier prediction for two situations, Fr 0.2 (figure 3.4A) and Fr 1.2 (figure 3.4B). This confusion matrix demonstrates a more detailed view into the prediction of the individual classes against the true values of these classes.

Table 3.3: Confusion matrix for different Fr, total accuracy, RE and PR. For classifier trained for 1 situation (Fr 0.0)

Froude number	Total accuracy (%)	RE (%)	PR (%)
0.0	96	93	93
0.2	89	94	80
0.4	61	96	28
0.6	66	96	28
0.8	66	99	44
1.0	62	98	34
1.2	43	99	23

The decrease in the overall performance of the classifier can be attributed to a decrease in performance to correctly predict water and vegetation from FR 0.2 and Fr 1.2 . For Fr 0.2 37.1% of the vegetation, pixels were predicted as plastic, this false prediction increased to 76% pixels for Fr 1.2. The prediction accuracy for water decreased even more sharply from 2.4% to 99.7% of pixels that were falsely predicted as plastic. At the same time, the percentage of false predictions of plastic as vegetation and water varied slightly comparing both situations. Furthermore, the prediction of vegetation and water as each other is negligible. This suggests that the index values of plastic do not change with higher Fr and the index values of vegetation and water converge toward plastic index values. Figure 3.5 shows the NDVI and NIDI values for varying Fr.

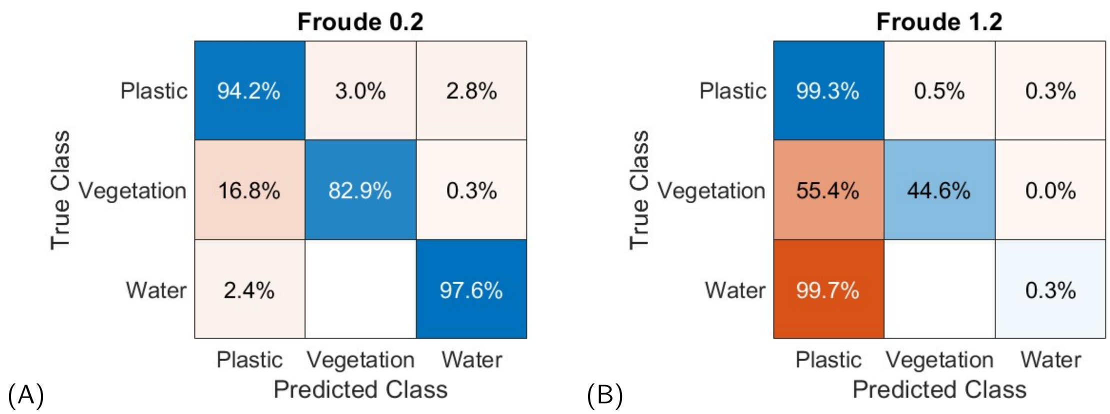

Figure 3.4: Normalized confusion matrix of the Naive Bayes classifier trained for Fr 0.0 and tested for Fr 0.2 (A) and Fr 1.2 (B). Empty cells have a value of 0, meaning that there is no pixel predicted that represents that cell.

The decrease in performance to detect vegetation is likely caused by submersion of the vegetation. The vegetation samples used are, due to the dimensions of the vegetation items used in the study, more susceptible to submersion by a rougher water flow than the plastic items used. Knaeps et al. (2021) found that submersion decreased the reflectance of an item. This leads to a decrease in the ratio between the specific wavelengths used to calculate NDVI and NIDI, and thus to a decrease in index values. Furthermore, the decrease in the performance to detect water is most likely caused by the change in spectral features of the water surface. For higher Fr the water surface roughness increases, which leads to a change in spectra reflectance (Hauer et al., 2022; Legleiter et al., 2017). This change in spectral reflectance leads to an increase in NDVI value for water.

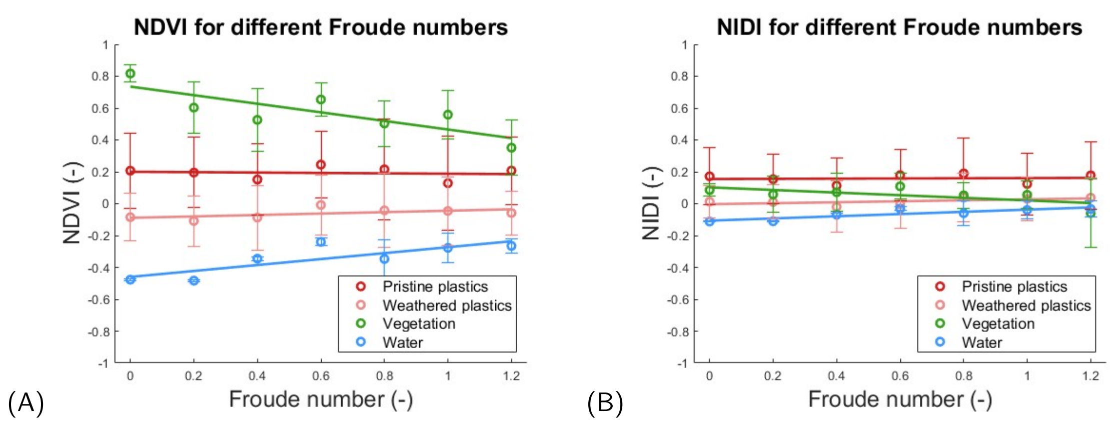

Figure 3.5: (A) mean, standard deviation and trend line of pristine and weathered plastics, vegetation and water NDVI values against Fr. (B) mean, standard deviation and trend line of pristine and weathered plastics, vegetation and water NIDI values against Fr.

3.3.1 Classifier trained for all data

In section 3.3 it is demonstrated that a change in Fr has a large influence on the performance of a classifier to detect plastic form vegetation and water. However this loss in accuracy is decreased by increasing the data set the classifier is trained on. Training the classifier for all data collected in this study decreases the loss in classifier accuracy with increasing Fr as is shown in table 3.4. Hereby, limiting the effect of Fr changes on the detectability of plastics from vegetation and water by the classifier. This is expected of a classifier that is trained on a data set with more variability. However, a decrease in the maximum accuracy of the classifier would have been expected because using a more variable data set leads to the range of values of a class being larger. Which could lead to more overlap between classes. Contrarily, the results show only a small decrease in maximum classifier accuracy. For Fr up to 1.0, values that represent the majority of rivers, the range of accuracy was 86-92%. Similar to previous classifier results the performance to predict plastic is lower than the overall accuracy of the classifier. The RE of plastic pixels is between 72% and 81%, and the PR is between 80% and 95%. The performance of the algorithm was slightly lower than the performance of algorithms used in previous studies. Iordache et al. (2022) found a plastic RE of 90 % and a PR of 94% with a random forest classifier for drone imagery. Similarly, Lavender (2022) determined a plastic RE of 89% for a classifier trained with Sentinel-2 imagery. The relatively high resolution could explain the reduced performance of the classifier used in this study compared to other studies. As Chen* et al. (2004) found that standard deviation is higher for finer resolutions, this causes a decrease in classifier performance. A counterargument is that the compared studies use more classes than the three that are used in this study. For instance in the study of Iordache et al. (2022) plastic are most often falsely predicted as bare soil and painted surface.

Table 3.4: Confusion matrix for different Fr, total accuracy, RE, PR, Classifier trained for total data-set

Froude number	Classifier accuracy	RE (%)	PR (%)
0.0	91	74	93
0.2	87	72	86
0.4	86	76	81
0.6	92	80	96
0.8	86	80	82
1.0	89	80	88
1.2	78	87	66

Figure 3.6 displays two normalized confusion matrices for Fr 0.2 (A) and Fr 1.2 (B). The classifier trained for all ambient conditions increased most in performance for the in the RE and PR of water pixels compared to the classifier trained for one ambient condition. The percentage of accurately predicted water is relatively stable with a decrease of only 4% from 100% to 96% true positive predictions. While the prediction performance to predict vegetation shows similar levels of decrease as the classifier trained for one circumstance (figure 3.4). This disparity between the increased performance of water prediction and the more stable performance of vegetation prediction by the classifier is probably caused by the data set characteristics. FR is one of the ambient conditions that was changed in the experiments. Making use of the whole data set to train the classifier increased the range of values the classifier labels as water. In contrast, vegetation was not a primary variable within the experiment. Changes in vegetation values occurred solely due to changes in ambient conditions. In a similar way, these ambient conditions affected plastic item values. This caused the vegetation range to increase considerably less than Fr values when the entire data set is used. Which leads to a decrease in the performance gain of the classifier train for the entire data set as well..

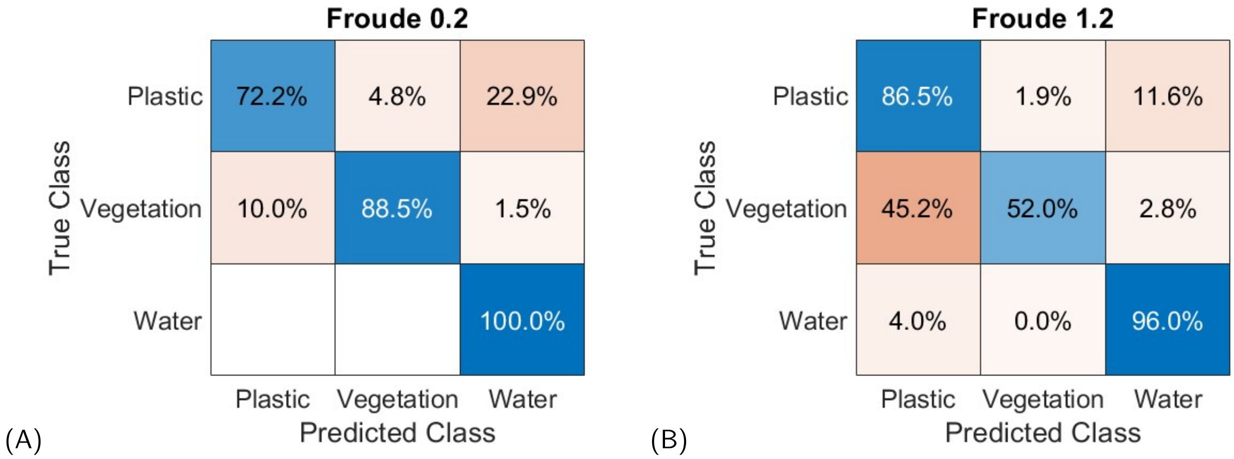

Figure 3.6: Normalized confusion matrix of the Naive Bayes classifier trained for the entire data-set and tested for Froude 0.2 (A) and Froude 1.2 (B). Empty cells have a value of 0, meaning that there is no pixel predicted that represents that cell.

3.4 Influence of plastic variability

The classifiers preformed better for detecting pristine plastics compared to weathered plastics. The difference in the performance of the classifier occured in the rate of correctly predicted plastics (RE), as can be seen in figure 3.7. The RE of pristine plastics is 85% (figure 3.7A) in comparison to 75% (figure 3.7 C) for weathered plastics. For weathered plastic, this extra 10% of plastic pixels is mostly predicted as water. The classifier predicted 17% of weathered plastic as water in comparison to only 8% of pristine plastics. In contrast, pristine and weathered plastic are predicted as vegetation at relatively similar rates, 6% and 9% respectively. The pristine plastics are thus easier to discriminate from water than weathered plastic by a Naive Bayes classifier. This is in agreement with the LDA results (figure 3.2) that had a larger difference for the separation of the plastics with water than for plastics with vegetation. A large difference in LDA weights at 842 nm was demonstrated for the LDA with water, causing a disparity in the ability to separate pristine and weathered plastic from water. The pristine plastic LDA was more than twice as large as that of weathered plastic and water, 0.35 and 0.15 respectively. The LDA at 665 nm, which was most important to separate plastic from vegetation, demonstrated smaller differences between pristine and weathered plastic. The LDA weight for pristine plastic was 0.27 compared to 0.33 for weathered plastic.

The conditions of plastic used to train an algorithm had limited influence on the performance of that classifier to discriminate plastic from vegetation and water. A pristine plastic data set had similar percentages of correctly predicted pixels for all classes, both for a classifier trained on pristine plastics (figure 3.7A) and a classifier trained on weathered plastics (3.7B). However the classifier trained on pristine plastic (figure 3.7D) decreased slightly, 5%, when it predicted weathered plastic in comparison to a classifier that was train for weathered plastic (figure 3.7C).

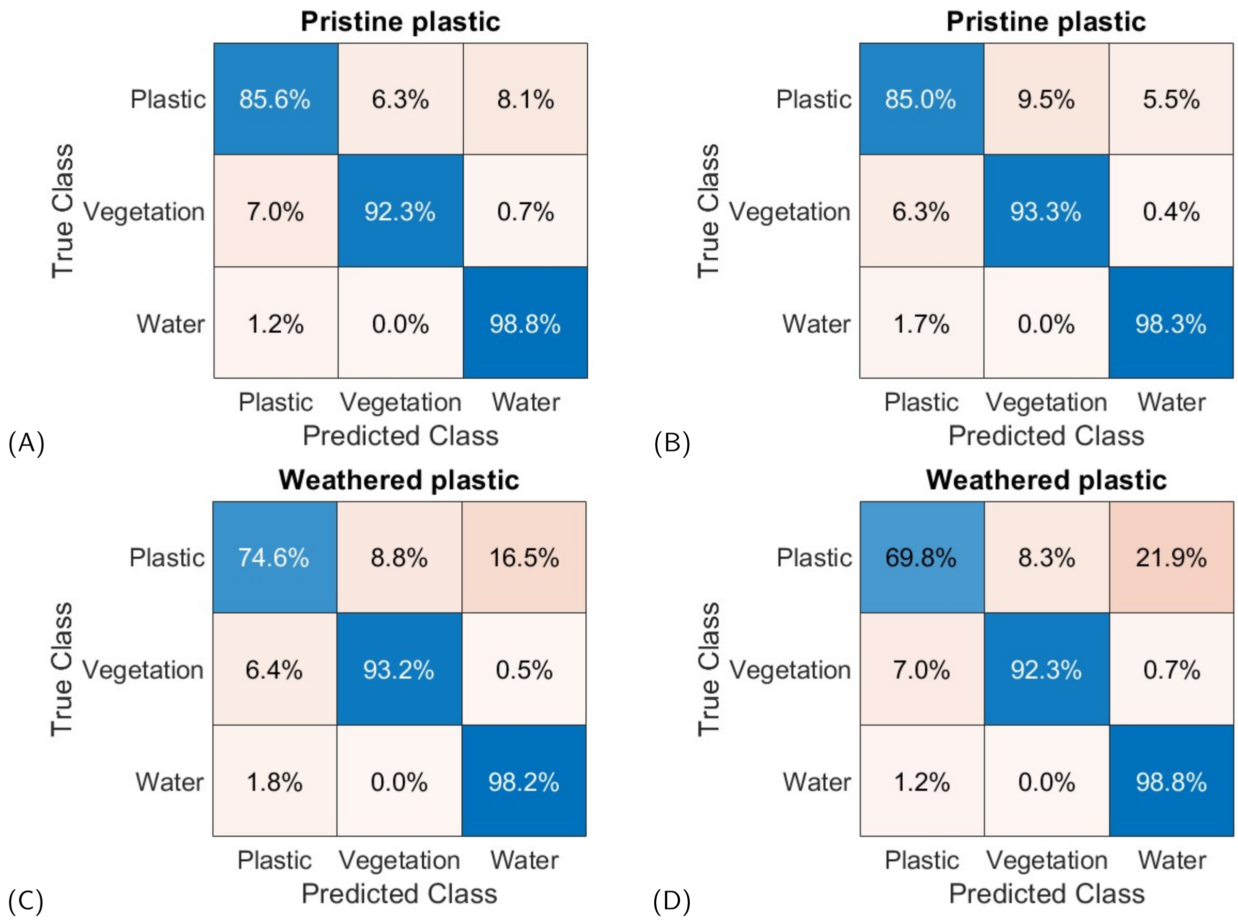

Figure 3.7: (A)Pristine plastic tested by a classifier trained on a pristine plastic data-set. (B)Pristine plastic tested by a classifier trained on a weathered plastic data-set. (C)weathered plastic tested by a classifier trained on a weathered plastic data-set. (D) Weathered plastic tested by a classifier trained on a pristine plastic data-set.

3.5 Synthesis and outlook

This study provides insights into the ability to detect macroplastics using multi-spectral remote sensing tools in the VIS-NIR range under various ambient conditions. Several studies have explored the plastic reflectance of macroplastics for imagery of varying spatial resolutions and wavelength ranges (Gnann et al., 2022). In this study red (665 nm), red-edge (740 nm), and near-infrared (842 nm) wavelengths were identified as important to discriminate plastic from vegetation. Similar wavelengths were identified by other studies(P. Tasseron et al., 2021; Topouzelis et al., 2021). Furthermore, it was indicated by the results that NDVI and PI were most suitable for plastic detection. yet, a combination of these indices with NIDI was proven to be 15% more accurate in the prediction plastic. Thereby, following the promising approach of combining spectral indices for plastic detection (Biermann et al., 2020).

As Gnann et al. (2022) stated in their review, external factors influencing the degree of reflections are wetting, submergence, and weathering. Also the light condition and the inherent and apparent optical properties of water are important to consider (Mishra et al., 2017). However their effects have not been researched on a large scale (Moshtaghi et al., 2021). This study investigated the spectral reflectance and detection under changing Fr of the water stream and incident light intensity and angles. From this selection of ambient conditions, changing Fr conditions had the most influence on the detectability of plastic. Furthermore, when the influence of ambient conditions was tested with a Naive

Bayes classifier a strong significant negative correlation was found between Fr and accuracy of the classifier. Even though spectral reflectance of the plastic itself was not effected by Fr, it changed the spectral reflectance of water and vegetation which converged the NDVI value range between plastic, vegetation and water. As a consequence, this decreased the ability to detect plastic, from vegetation and water. Biermann et al. (2020) saw similar effects on the functionality of algorithms with increasing water turbidity levels, as that also caused higher NDVI values of the water. Simultaneously, the vegetation was more susceptible to waves than plastic items, due to its dimensions. An increase in water roughness attributed to the submergence of vegetation, and thereby lowered the spectral reflectance of vegetation (Moshtaghi et al., 2021). The other variables, light intensity, light angle and the condition of the plastic seemed to have less influence on the ability to discriminate plastic from vegetation and water. But more investigation into the effect of these factors is needed to conclude that their effects are negligible.

A major limitation of this research is that it mostly has been conducted in a laboratory environment under artificial lighting. In natural environments, the detection and identification of macroplastics is influenced by external factors not taken into account, such as submergence, water turbidity, and atmospheric effects (Gnann et al., 2022). P. F. Tasseron et al. found a smaller range of reflectance intensity of plastic and vegetation comparing lab and field measurements, which they contributed to rapidly differing light conditions. Secondly, plastic was in this research compared to water and vegetation. Other items commonly found near riverine systems, items such as non-plastic waste, wood, and water turbidity and color (Biermann et al., 2020; Iordache et al., 2022), were excluded. This complicates the translation of these results into natural environments. A third limitation is the range of wavelengths used in this study. Most studies that used spectral indices to detect floating plastics used wavelength up to 2500 nm (Garaba and Dierssen, 2018; Topouzelis et al., 2021) which are deemed more suitable for plastic detection (**empty citation**). However, the classifier for NDVI + NIDI used in this study had similar effectivity to correctly predict plastic (81%) as classifiers used by (Acuña-Ruz et al., 2018; Sannigrahi et al., 2022), which predicted 70-90% of the plastic correctly.

The findings of this study enable future research in several directions. This research should focus on ambient factors that simultaneously effect a only part of the objects scanned in riverine or marine environments. For example, this study found Fr to have the larger influence on the effectivity to discriminate plastic, vegetation and water. However the change in FR did not influence the reflectance of plastic itself, only the reflectance of vegetation and water. Therefore causing a divergence in the range of NDVI values of all three classes, and subsequently an overprediction of plastic. Other ambient conditions that lead to changes in spectral reflectance and detectability of plastic items were found previously due to submergence and turbidity of the water (Garaba and Harmel, 2022; Knaeps et al., 2021). All three ambient variables, Fr, submergence of plastic and turbidity, influence the spectral reflectance of one object class, causing the ratio of index values to change between different object classes. Further research is needed to properly asses the impact of these ambient conditions on the detection of plastic objects in riverine and marine environments.

Furthermore, a study into the effect of Fr can be conducted in natural environments. The floating characteristics of plastic items in rivers can be different than observed in a laboratory environment. For example, the plastic items occur mostly floating on top of the water in the flume, while plastic items have been found floating (partially) submerged in natural environments (van Emmerik and Schwarz, 2020). Furthermore this study provided a promising method, a combination of spectral indices NDVI and NIDI, to detect plastic items from vegetation and water. This method can be used for close range multispectral analysis and space borne analysis utilising Sentinel-2 sensors of floating plastics.

4 | Conclusions

This study provides a database of multi-spectral imagery of plastics and vegetation under multiple ambient conditions. As well as an analysis of the effect of ambient conditions on the ability to distinguish plastic pixels from vegetation and water. Based on the analysis and discussion the following conclusion can be drawn:

- Froude numbers changes were found to have a high negative and significant correlation (Pearson's r=-0.92) with the accuracy of a Naive Bayes classifier. Suggesting that Froude number changes within the range most commonly in riverine systems have a considerable impact on the ability to discriminate plastic from vegetation and water. Future studies exploring the effects of ambient conditions on remote sensing of macroplastics can build upon this knowledge.

- The importance of each of the nine wavelength bands of the MAIA-S2 sensor is showed by conducting linear discriminant analyses of the reflectance values of plastic, water and vegetation. High LDA weights were found at bands B4 (665 nm), B6 (740 nm) and B8 (842 nm), indicating which component of spectral indices perform best. However, Pristine plastics had a higher LDA weights for the separation than weathered plastics, suggesting that they can be discriminated more efficiently.

- Using a combination of NDVI and NIDI is a promising approach for the ability to distinguish plastics, vegetation and water. Training a classifier using both NDVI and NIDI improved the accuracy with 5% point to 91% in comparison to a NDVI trained classifier and improving the plastic RE with 15% point to 81%.

- The classifier showed similar levels of performance for detecting weathered plastic, when trained for pristine plastic as for weathered plastic with the RE decreasing 5%. This suggests that the plastic conditions tested possibly have limited influence on the detectability of plastic form vegetation and water, but more research into this is needed to test for macroplastic various databases.

- The classifier performed better when predicted pristine plastic than weathered plastics, the RE for pristine plastics was 86% against 74% for weathered plastic. This would suggest that pristine plastics can be more effectively discriminated than weathered plastics from vegetation and water.

Acknowledgements

I would like to thank my supervisors, Tim van Emmerik and Louise Schreyers for their support to this thesis. Their constructive feedback and recommendations have helped me along the way to shape this thesis. I would also like to thank Paolo Tasseron for his enthusiastic support and expert guidance. next, I would like to thank David Boelee for preparing the setup of the tilting flume and for his guidance during the experiments. Lastly, I want to thank the HWM-students from the thesis ring for their feedback and support.

Bibliography

Acuña-Ruz, T., Uribe, D., Taylor, R., Amézquita, L., Guzmán, M. C., Merrill, J., Martınez, P., Voisin, L., & Mattar, C. (2018). Anthropogenic marine debris over beaches: Spectral characterization for remote sensing applications. *Remote Sensing of Environment*, *217*, 309–322.

Al-Zawaidah, H., Ravazzolo, D., & Friedrich, H. (2021). Macroplastics in rivers: Present knowledge, issues and challenges. *Environmental Science: Processes & Impacts*, *23*(4), 535–552.

Andriolo, U., Garcia-Garin, O., Vighi, M., Borrell, A., & Gonçalves, G. (2022). Beached and floating litter surveys by unmanned aerial vehicles: Operational analogies and differences. *Remote Sensing*, *14*(6), 1336.

Andriolo, U., Gonçalves, G., Sobral, P., & Bessa, F. (2021). Spatial and size distribution of macro-litter on coastal dunes from drone images: A case study on the atlantic coast. *Marine Pollution Bulletin*, *169*, 112490.

Balsi, M., Moroni, M., Chiarabini, V., & Tanda, G. (2021). High-resolution aerial detection of marine plastic litter by hyperspectral sensing. *Remote Sensing*, *13*(8), 1557.

Barboza, L. G. A., Cózar, A., Gimenez, B. C., Barros, T. L., Kershaw, P. J., & Guilhermino, L. (2019). Macroplastics pollution in the marine environment. In *World seas: An environmental evaluation* (pp. 305–328). Elsevier.

Best, J. (2019). Anthropogenic stresses on the world's big rivers. *Nature Geoscience*, *12*(1), 7–21.

Biermann, L., Clewley, D., Martinez-Vicente, V., & Topouzelis, K. (2020). Finding plastic patches in coastal waters using optical satellite data. *Scientific reports*, *10*(1), 1–10.

Blettler, M., Ulla, M. A., Rabuffetti, A. P., & Garello, N. (2017). Plastic pollution in freshwater ecosystems: Macro-, meso-, and microplastic debris in a floodplain lake. *Environmental monitoring and assessment*, *189*(11), 1–13.

Bruge, A., Barreau, C., Carlot, J., Collin, H., Moreno, C., & Maison, P. (2018). Monitoring litter inputs from the adour river (southwest france) to the marine environment. *Journal of Marine Science and Engineering*, *6*(1), 24.

Chen*, D., Stow, D., & Gong, P. (2004). Examining the effect of spatial resolution and texture window size on classification accuracy: An urban environment case. *International Journal of Remote Sensing*, *25*(11), 2177–2192.

Ciappa, A. C. (2021). Marine plastic litter detection offshore hawai'i by sentinel-2. *Marine Pollution Bulletin*, *168*, 112457.

Corbari, L., Maltese, A., Capodici, F., Mangano, M., Sarà, G., & Ciraolo, G. (2020). Indoor spectroradiometric characterization of plastic litters commonly polluting the mediterranean sea: Toward the application of multispectral imagery. *Scientific Reports*, *10*(1), 1–12.

Cortesi, I., Masiero, A., De Giglio, M., Tucci, G., & Dubbini, M. (2021). Random forest-based river plastic detection with a handheld multispectral camera. *The International Archives of Photogrammetry, Remote Sensing and Spatial Information Sciences*, *43*, 9–14.

Cortesi, I., Masiero, A., Tucci, G., & Topouzelis, K. (2022). Uav-based river plastic detection with a multispectral camera. *The International Archives of Photogrammetry, Remote Sensing and Spatial Information Sciences*, *43*, 855–861.

Dierssen, H. M. (2019). Hyperspectral measurements, parameterizations, and atmospheric correction of whitecaps and foam from visible to shortwave infrared for ocean color remote sensing. *Frontiers in Earth Science*, *7*, 14.

Dobbin, K. K., & Simon, R. M. (2011). Optimally splitting cases for training and testing high dimensional classifiers. *BMC medical genomics*, *4*(1), 1–8.

ElMasry, G., & Sun, D.-W. (2010). Principles of hyperspectral imaging technology. In *Hyperspectral imaging for food quality analysis and control* (pp. 3–43). Elsevier.

engineering SRL; Eoptis SRL; Fondazione Bruno Kessler, S. (2017). *Maia-s2*. Retrieved January 16, 2023, from https://sentinels.copernicus.eu/web/sentinel/technical-guides/sentinel-2-msi/msi-instrument

Erni-Cassola, G., Zadjelovic, V., Gibson, M. I., & Christie-Oleza, J. A. (2019). Distribution of plastic polymer types in the marine environment; a meta-analysis. *Journal of hazardous materials*, *369*, 691–698.

Ferrick, M. G. (1985). Analysis of river wave types. *Water Resources Research*, *21*(2), 209–220.

Fisher, R. A. (1936). The use of multiple measurements in taxonomic problems. *Annals of eugenics*, *7*(2), 179–188.

Freeze, B., Smolentsev, S., Morley, N., & Abdou, M. (2003). Characterization of the effect of froude number on surface waves and heat transfer in inclined turbulent open channel water flows. *International journal of heat and mass transfer*, *46*(20), 3765–3775.

Gall, S. C., & Thompson, R. C. (2015). The impact of debris on marine life. *Marine pollution bulletin*, *92*(1-2), 170–179.

Garaba, S. P., Arias, M., Corradi, P., Harmel, T., de Vries, R., & Lebreton, L. (2021). Concentration, anisotropic and apparent colour effects on optical reflectance properties of virgin and ocean-harvested plastics. *Journal of Hazardous Materials*, *406*, 124290.

Garaba, S. P., & Dierssen, H. M. (2018). An airborne remote sensing case study of synthetic hydrocarbon detection using short wave infrared absorption features identified from marine-harvested macro-and microplastics. *Remote Sensing of Environment*, *205*, 224–235.

Garaba, S. P., & Dierssen, H. M. (2020). Hyperspectral ultraviolet to shortwave infrared characteristics of marine-harvested, washed-ashore and virgin plastics. *Earth System Science Data*, *12*(1), 77–86.

Garaba, S. P., & Harmel, T. (2022). Top-of-atmosphere hyper and multispectral signatures of submerged plastic litter with changing water clarity and depth. *Optics Express*, *30*(10), 16553–16571.

Gasperi, J., Dris, R., Bonin, T., Rocher, V., & Tassin, B. (2014). Assessment of floating plastic debris in surface water along the seine river. *Environmental pollution*, *195*, 163–166.

Gnann, N., Baschek, B., & Ternes, T. (2022). Close-range remote sensing-based detection and identification of macroplastics on water assisted by artificial intelligence: A review. *Water Research*, 118902.

Hauer, F. R., Lorang, M. S., & Gonser, T. (2022). Remote sensing to characterize river floodplain structure and function. *Remote Sensing*, *14*(5), 1132.

Hu, C. (2009). A novel ocean color index to detect floating algae in the global oceans. *Remote Sensing of Environment*, *113*(10), 2118–2129.

Iordache, M.-D., De Keukelaere, L., Moelans, R., Landuyt, L., Moshtaghi, M., Corradi, P., & Knaeps, E. (2022). Targeting plastics: Machine learning applied to litter detection in aerial multispectral images. *Remote Sensing*, *14*(22), 5820.

Kikaki, A., Karantzalos, K., Power, C. A., & Raitsos, D. E. (2020). Remotely sensing the source and transport of marine plastic debris in bay islands of honduras (caribbean sea). *Remote Sensing*, *12*(11), 1727.

Knaeps, E., Sterckx, S., Strackx, G., Mijnendonckx, J., Moshtaghi, M., Garaba, S. P., & Meire, D. (2021). Hyperspectral-reflectance dataset of dry, wet and submerged marine litter. *Earth System Science Data*, *13*(2), 713–730.

Lavender, S. (2022). Detection of waste plastics in the environment: Application of copernicus earth observation data. *Remote Sensing*, *14*(19), 4772.

Lebreton, L., Slat, B., Ferrari, F., Sainte-Rose, B., Aitken, J., Marthouse, R., Hajbane, S., Cunsolo, S., Schwarz, A., Levivier, A., et al. (2018). Evidence that the great pacific garbage patch is rapidly accumulating plastic. *Scientific reports*, *8*(1), 1–15.

Legleiter, C. J., Mobley, C. D., & Overstreet, B. T. (2017). A framework for modeling connections between hydraulics, water surface roughness, and surface reflectance in open channel flows. *Journal of Geophysical Research: Earth Surface*, *122*(9), 1715–1741.

Leung, K. M. (2007). Naive bayesian classifier. *Polytechnic University Department of Computer Science/Finance and Risk Engineering*, *2007*, 123–156.

Li, C., & Wang, B. (2014). Fisher linear discriminant analysis. *CCIS Northeastern University*.

Liu, H. Q., & Huete, A. (1995). A feedback based modification of the ndvi to minimize canopy background and atmospheric noise. *IEEE transactions on geoscience and remote sensing*, *33*(2), 457–465.

Martınez-Vicente, V., Clark, J. R., Corradi, P., Aliani, S., Arias, M., Bochow, M., Bonnery, G., Cole, M., Cózar, A., Donnelly, R., et al. (2019). Measuring marine plastic debris from space: Initial assessment of observation requirements. *Remote Sensing*, *11*(20), 2443.

McIlgorm, A., Campbell, H. F., & Rule, M. J. (2011). The economic cost and control of marine debris damage in the asia-pacific region. *Ocean & Coastal Management*, *54*(9), 643–651.

Meacham-Hensold, K., Montes, C. M., Wu, J., Guan, K., Fu, P., Ainsworth, E. A., Pederson, T., Moore, C. E., Brown, K. L., Raines, C., et al. (2019). High-throughput field phenotyping using hyperspectral reflectance and partial least squares regression (plsr) reveals genetic modifications to photosynthetic capacity. *Remote sensing of environment*, *231*, 111176.

Mihai, F.-C. (2018). Rural plastic emissions into the largest mountain lake of the eastern carpathians. *Royal Society Open Science*, *5*(5), 172396.

Mishra, D. R., Ogashawara, I., & Gitelson, A. A. (2017). *Bio-optical modeling and remote sensing of inland waters*. Elsevier.

Mobley, C. D. (1999). Estimation of the remote-sensing reflectance from above-surface measurements. *Applied optics*, *38*(36), 7442–7455.

Moshtaghi, M., Knaeps, E., Sterckx, S., Garaba, S., & Meire, D. (2021). Spectral reflectance of marine macroplastics in the vnir and swir measured in a controlled environment. *Scientific Reports*, *11*(1), 1–12.

Nakayama, A., & Yokojima, S. (2001). Direct numerical simulation of the fully developed open-channel flow at subcritical froude numbers.

perClass BV. (n.d.). *Perclass toolbox*. Retrieved January 16, 2023, from https://sentinels.copernicus.eu/web/sentinel/technical-guides/sentinel-2-msi/msi-instrument

Picard, R. R., & Berk, K. N. (1990). Data splitting. *The American Statistician*, *44*(2), 140–147.

PlasticsEurope. (2022). *Plastics—the facts 2022. an analysis of european plastics production, demand and waste data* (tech. rep.). PlasticsEurope.

Rech, S., Macaya-Caquilpán, V., Pantoja, J., Rivadeneira, M., Madariaga, D. J., & Thiel, M. (2014). Rivers as a source of marine litter–a study from the se pacific. *Marine pollution bulletin*, *82*(1-2), 66–75.

Rokni, K., Ahmad, A., Selamat, A., & Hazini, S. (2014). Water feature extraction and change detection using multitemporal landsat imagery. *Remote sensing*, *6*(5), 4173–4189.

Rouse, J., Haas, R., Schell, J., & Deering, D. (1974). Monitoring vegetation systems in the great plains with erts in proc. *ERTS-1 Symposium 3rd, Greenbelt, Washington, NASA*.

Sannigrahi, S., Basu, B., Basu, A. S., & Pilla, F. (2022). Development of automated marine floating plastic detection system using sentinel-2 imagery and machine learning models. *Marine Pollution Bulletin*, *178*, 113527.

Sentinel-2, C. (n.d.). *Sentinel-2 msi technical guide - multispectral instrument (msi) overview*. Retrieved January 16, 2023, from https://sentinels.copernicus.eu/web/sentinel/technical-guides/sentinel-2-msi/msi-instrument

Tasseron, P., Van Emmerik, T., Peller, J., Schreyers, L., & Biermann, L. (2021). Advancing floating macroplastic detection from space using experimental hyperspectral imagery. *Remote Sensing*, *13*(12), 2335.

Tasseron, P. F., Schreyers, L., Peller, J., Biermann, L., & van Emmerik, T. (2022). Toward robust river plastic detection: Combining lab and field-based hyperspectral imagery. *Earth and Space Science*, *9*(11), e2022EA002518.

The MathWorks, I. (2013). *Classificationnaivebayes*. http://https://nl.mathworks.com/help/stats/classificationnaivebayes.html

Themistocleous, K., Papoutsa, C., Michaelides, S., & Hadjimitsis, D. (2020). Investigating detection of floating plastic litter from space using sentinel-2 imagery. *Remote Sensing*, *12*(16), 2648.

Topouzelis, K., Papageorgiou, D., Karagaitanakis, A., Papakonstantinou, A., & Arias Ballesteros, M. (2020). Remote sensing of sea surface artificial floating plastic targets with sentinel-2 and unmanned aerial systems (plastic litter project 2019). *Remote Sensing*, *12*(12), 2013.

Topouzelis, K., Papageorgiou, D., Suaria, G., & Aliani, S. (2021). Floating marine litter detection algorithms and techniques using optical remote sensing data: A review. *Marine Pollution Bulletin*, *170*, 112675.

Topouzelis, K., Papakonstantinou, A., & Garaba, S. P. (2019). Detection of floating plastics from satellite and unmanned aerial systems (plastic litter project 2018). *International Journal of Applied Earth Observation and Geoinformation*, *79*, 175–183.

Van Emmerik, T., Kieu-Le, T.-C., Loozen, M., Van Oeveren, K., Strady, E., Bui, X.-T., Egger, M., Gasperi, J., Lebreton, L., Nguyen, P.-D., et al. (2018). A methodology to characterize riverine macroplastic emission into the ocean. *Frontiers in Marine Science*, *5*, 372.

van Calcar, C. v., & van Emmerik, T. v. (2019). Abundance of plastic debris across european and asian rivers. *Environmental Research Letters*, *14*(12), 124051.

van Emmerik, T., & Schwarz, A. (2020). Plastic debris in rivers. *Wiley Interdisciplinary Reviews: Water*, *7*(1), e1398.

Vescovo, L., Wohlfahrt, G., Balzarolo, M., Pilloni, S., Sottocornola, M., Rodeghiero, M., & Gianelle, D. (2012). New spectral vegetation indices based on the near-infrared shoulder wavelengths for remote detection of grassland phytomass. *International journal of remote sensing*, *33*(7), 2178–2195.

A | Appendix

A.1 Overview of plastic items and pixels in database

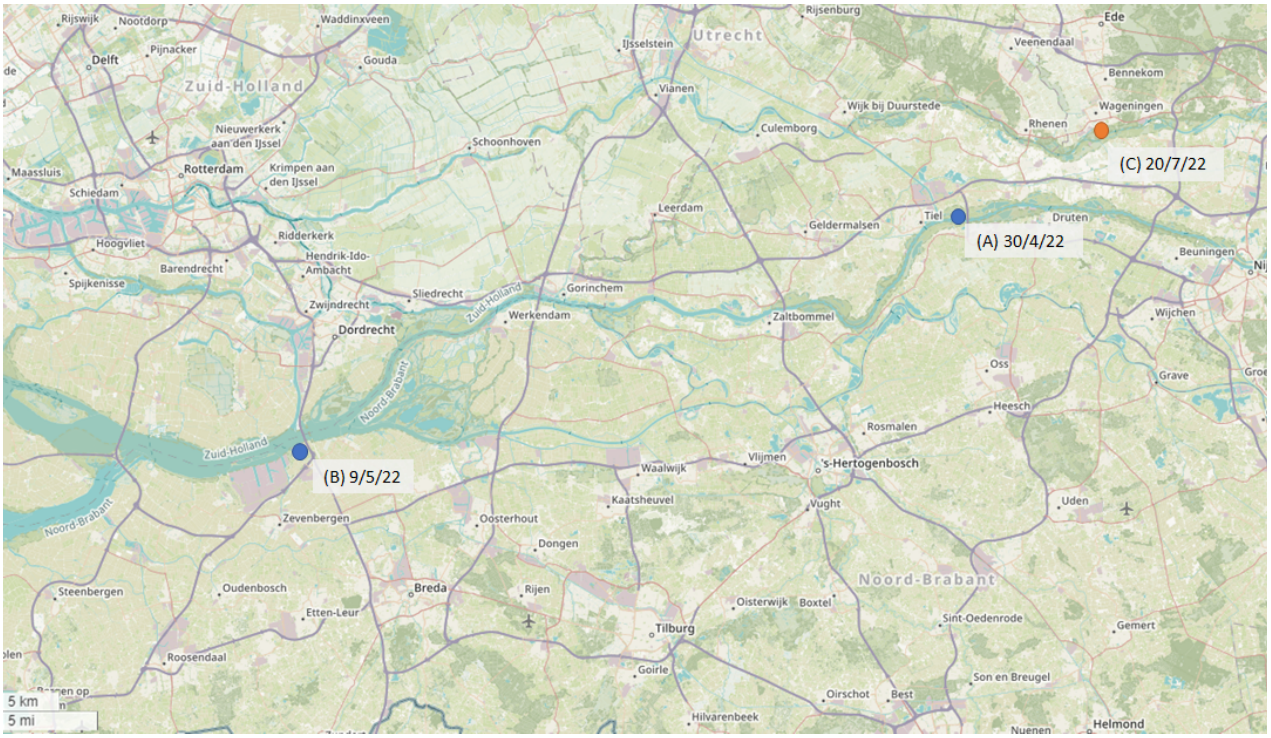

Figure A.1: An overview of the locations where the plastic (A B) and vegetation (C) is collected. The collection date is attached to the locations on the map.

A.2 Classifier performance for different indices

Table A.1: Correlation between ambient conditions and NDVI-NIDI trained Naive Bayes classifier, including inside and outside measurements for illumination (Dry)

Ambient condition	Pearson correlation r	Pearson correlation p	Spearman correlation r	Spearman correlation p
Froude number	-0.92	<0.01	-0.96	<0.01
Illumination (Wet)	-0.53	0.36	0.00	1.0
Illumination (Dry)	-0.76	0.08	-0.6	0.24
Light angle	-0.58	0.42	-0.8	0.33
Illumination (Dry inside)	0.99	0.06	1.00	0.33
Illumination (Dry outside)	0.62	0.57	0.50	1.00

A.3 Classifier performance for different indices

Index	Accuracy	Plastic		Vegetation		Water	
		RE	PR	RE	PR	RE	PR
9 Bands	79	48	83	92	80	98	77
NDVI	86	66	90	93	81	99	88
EVI	33	0	100	100	33	0	0
PI	86	66	90	92	81	99	88
NIDI	67	26	76	89	57	86	78
NDSI	44	21	64	25	56	86	39
NDWI	72	39	74	81	82	96	65
NDVI_NIDI	91	81	92	99	91	93	88
NDVI_NDWI	96	67	88	91	81	99	90

Table A.2: Confusion matrix for classifier trained for different indices. The total classifier accuracy and RE and PR for the three classes, plastic, vegetation and water is depicted in percentages.

A.4 Classifier performance, single circumstance trained

Ambient Condition	Accuracy	Plastic		Vegetation		Water	
		RE	PR	RE	PR	RE	PR
Fr 0.0*	92	74	89	97	92	99	96
Fr 0.2	87	79	79	84	84	98	98
Fr 0.4	58	83	26	81	87	0	0
Fr 0.6	61	77	23	89	79	0	5
Fr 0.8	61	82	39	75	74	23	100
Fr 1.0	54	93	32	68	85	1	86
Fr 1.2	45	80	20	56	69	0	67
Wet 600 Lumen**	87	70	98	0	0	99	97
Wet 900 Lumen*	90	72	84	93	87	99	97
Wet 1200 Lumen	91	75	88	93	87	99	97
Wet 1500 Lumen	92	71	92	98	91	99	97
Wet 1800 Lumen	73	74	50	90	74	52	96
Dry 600 Lumen*	82	80	85	84	78		
Dry 900 Lumen	86	84	92	89	79		
Dry 1200 Lumen	89	88	92	91	87		
Dry 22500 Lumen	85	72	100	100	72		
Dry 45000 Lumen	81	65	100	100	70		
Dry 95000 Lumen	79	61	100	64	100		
Light angle 60° *	91	84	95	96	88		
Light angle 70°	89	81	95	96	84		
Light angle 80°	86	85	91	88	79		
Light angle 90°	89	85	91	92	86		

Table A.3: Confusion matrix for different Fr numbers. The total classifier accuracy and RE and PR for the three classes, plastic, vegetation and water is depicted in percentages. For a classifier trained for 1 situation. For variables dry illumination and light angle, water was not taken into account. *Data set classifier is trained on. **Classifier not trained for WET600, because of the corruption of vegetation imagery for the WET600 situation

A.5 Classifier performance, trained on all circumstances

Ambient condition	Accuracy	Plastic RE	Plastic PR	Vegetation RE	Vegetation PR	Water RE	Water PR
Fr 0.0	91	74	93	98	98	100	86
Fr 0.2	87	72	86	88	96	100	89
Fr 0.4	86	76	81	83	97	100	90
Fr 0.6	92	80	96	96	94	100	94
Fr 0.8	86	80	82	86	94	94	89
Fr 1.0	89	80	88	88	93	97	91
Fr 1.2	78	87	66	53	95	96	95
Wet 900 Lumen	88	78	88	94	96	100	90
Wet 1200 Lumen	89	75	89	93	97	100	81
Wet 1800 Lumen	92	81	97	96	96	100	89
Dry 600 Lumen	88	90	89	86	93		
Dry 900 Lumen	92	94	94	89	94		
Dry 1200 Lumen	92	91	94	94	97		
Dry 22500 Lumen	87	75	100	100	75		
Dry 45000 Lumen	83	66	100	100	72		
Dry 95000 Lumen	80	60	100	100	63		
Light angle 60	96	93	99	99	97		
Light angle 70	96	93	99	99	96		
Light angle 90	95	91	99	99	96		

Table A.4: Confusion matrix for different Fr numbers. The total classifier accuracy and RE and PR for the three classes, plastic, vegetation and water is depicted in percentages. For a classifier trained for all data. For variables dry illumination and light angle, water was not taken into account.